J. theor. Biol. (1978) **71**, 401–420

Bifurcation of Periodic Solutions of the Hodgkin–Huxley Model for the Squid Giant Axon

BRIAN HASSARD

Department of Mathematics, State University of New York at Buffalo, New York, U.S.A.

(*Received* 15 *February* 1977, *and in revised form* 3 *October* 1977)

The Hodgkin–Huxley model of the space-clamped squid giant axon is shown to admit unstable periodic solutions for current stimuli less than the stimulus at which the rest state becomes linearly unstable. The periodic solutions are demonstrated both by bifurcation theory and by numerical integration. The presence of subcritical unstable oscillations explains the discontinuous behaviour of the amplitude of the repetitive response as a function of current stimulus

1. Introduction

It has been long known (Hodgkin & Huxley, 1952), (Sabah & Spangler, 1970) that over a range of current stimuli I, the Hodgkin–Huxley model for the space-clamped squid giant axon responds repetitively, i.e. admits periodic solutions. The range of stimuli found is $I_0 < I < I_2$, where, at 6·3°C, $I_0 \approx 6{\cdot}2$ μA cm^{-2} and $I_2 \approx 154$ μA cm^{-2}. If the current stimulus I is increased by steps, stable large amplitude periodic solutions suddenly appear for $I \geq I_0$.

Linear stability analysis, however, shows that the rest state is stable for $I < I_1$, where $I_1 \approx 9{\cdot}8$ μA cm^{-2} at 6·3°C. Indeed, if the current stimulus is increased very slowly, the appearance of the large amplitude oscillations may be postponed until $I \approx I_1$.

Recently, Troy (1974) used bifurcation theory to prove that small amplitude oscillations exist for $I \approx I_1$, in precisely one of the cases $I < I_1$, $I = I_1$, $I > I_1$. The question, which one of these cases actually applies, was left unresolved.

In this paper, we use a combination of bifurcation theory and numerical integration to investigate the four bifurcation points I_0, I_1, I_2 and I_3, where I_3 represents a new, unstable–unstable bifurcation, $I_0 < I_3 < I_1$.

For $I \approx I_0$, $I > I_0$, there is a large amplitude unstable periodic oscillation in addition to the usual large stable oscillation. As $I \to I_0$, this pair of large

0022-5193/78/0406-0401 $02.00/0

amplitude solutions coalesces into a single solution for which two characteristic exponents vanish and two are negative. This single solution marks the first repetitive behaviour of the Hodgkin–Huxley model.

For $I \approx I_1$, $I < I_1$, there is a small amplitude unstable periodic solution in addition to the large stable solution. As $I \to I_1$, the amplitude of the unstable solution tends to zero. Although this small solution is not physically observable, it is of interest in that it represents the mechanism whereby small deviations from the rest state grow into larger amplitude oscillations.

For $I \approx I_2$, $I < I_2$, bifurcation theory predicts precisely the same family of small amplitude stable oscillations computed previously. It should be noted that bifurcation theory correctly predicts both the square root behaviour of the amplitude and the linear behaviour of the period.

For $I \approx I_3$, $I > I_3$ where, at 6·3°C, $I_3 = 7{\cdot}8466$, there are a pair of medium amplitude ($v_{pp} \approx 16{\cdot}17$) unstable oscillations in addition to the large amplitude stable oscillation. As $I \to I_3$, this pair of solutions coalesces into a single solution for which two characteristic exponents vanish, one is positive and one negative. The existence of the point I_3 strongly suggests that there is a second unstable–unstable bifurcation at some point $I = I_4$, $I_4 > I_3$.

This paper is the first application to the Hodgkin–Huxley system of a numerical scheme capable of computing unstable periodic solutions, is one of the most complex application of bifurcation formulae to date, and is the first application of Wan's formula for τ_2 (Hassard & Wan, 1977).

Our material is organized as follows. In section 2, we describe the current-clamped Hodgkin–Huxley system and its stationary point. Enough bifurcation theory to explain our results is given in section 3. Section 4 presents the results (both bifurcation theoretic and numerical) at the point $I = I_1$ while section 5 presents the corresponding results for $I = I_2$. Section 6, describes the large amplitude bifurcation at $I = I_0$ and explains why the exchange of stabilities occurs at a point of vertical tangency of the bifurcation diagram. Section 7 investigates the unstable–unstable bifuraction at $I = I_3$, and section 8 is a general discussion of the results. Details of the bifurcation analytic calculation and the formulae employed are given in appendices A and B, while the numerical schemes are described in appendix C.

2. The Current Clamped Hodgkin–Huxley System

As is customary, we define:

$$G(v, m, n, h) = 36n^4(v-12)+120m^3h(v+115)+0{\cdot}3(v+10.599),$$

where the variables v, m, n and h represent (respectively) voltage in mv, sodium activation, potassium activation and sodium inactivation. We use

the Hodgkin–Huxley values for the measured conductances and rest potentials from the outset for convenience. The original rate "constants" for 6·3°C are:

$$\alpha_m(v) = 1/\text{expc}\,(v_{25}), \qquad \beta_m(v) = 4\exp(v/18),$$
$$\alpha_n(v) = 0{\cdot}1/\text{expc}\,(v_{10}), \qquad \beta_n(v) = \exp(v/80)/8,$$
$$\alpha_h(v) = 0{\cdot}07\exp(v/20), \qquad \beta_h(v) = 1/[1+\exp(v_{30})],$$

where:

$$v_{10} = (v+10)/10, \quad v_{25} = (v+25)/10, \quad v_{30} = (v+30)/10,$$

and expc is the function:

$$\text{expc}\,(x) = \begin{cases}(e^x-1)\,x, & x \neq 0\\ 1, & x = 0.\end{cases}$$

With the temperature compensation factor $\phi = 3^{(T-6\cdot3)/10}$, with the membrane capacitance set equal to $1\mu\text{f cm}^{-2}$, the current stimulus I measured in $\mu\text{A cm}^{-2}$ and the time variable t in ms, the current clamped Hodgkin–Huxley system is:

$$\begin{aligned}\frac{dv}{dt} &= -I-G,\\ \frac{dm}{dt} &= [(1-m)\alpha_m(v)-m\beta_m(v)]\phi\\ \frac{dn}{dt} &= [(1-n)\alpha_n(v)-n\beta_n(v)]\phi\\ \frac{dh}{dt} &= [(1-h)\alpha_h(v)-h\beta_h(v)]\phi,\end{aligned} \tag{1}$$

or

$$\frac{d\mathbf{x}}{dt} = \mathbf{f}(\mathbf{x}, I),$$

where

$$\mathbf{x} = (v, m, n, h)^t$$

and $\mathbf{f}$ is the vector-valued function defined by the right-hand side of equation (1).

(A) THE STATIONARY POINT

Any stationary point:

$$\mathbf{x}_* = (v_*, m_*, n_*, h_*)^t,$$

must satisfy:

$$m_* = m_\infty(v_*), \quad n_* = n_\infty(v_*), \quad h_* = h_\infty(v_*),$$

where:

$$m_\infty(v) = \alpha_m(v)/[\alpha_m(v)+\beta_m(v)],$$
$$n_\infty(v) = \alpha_n(v)/[\alpha_n(v)+\beta_n(v)],$$

and

$$h_\infty(v) = \alpha_h(v)/[\alpha_h(v)+\beta_h(v)].$$

The "v" equation then implies:

$$g(v_*)+I = 0,$$

where:

$$g(v) = G(v, m_\infty(v), n_\infty(v), h_\infty(v)).$$

The function g (the steady state $I-v$ relation) is monotonic increasing, so that both $v_* = g^{-1}(-I)$ and $\mathbf{x}_* = \mathbf{x}_*(I)$ are uniquely determined once I is specified.

The stability of the stationary point $\mathbf{x}_*$ as a solution of (1) varies with I. The eigenvalues of the Jacobian matrix:

$$J_*(I) = \frac{\partial f^i}{\partial x_j}(\mathbf{x}_*; I),$$

for $\phi = 1$ are given in Table 1 as functions of I. For $I < 9{\cdot}78$ and for $I > 154{\cdot}5$, the eigenvalues all have negative real parts so the stationary point is linearly stable. For $9{\cdot}78 < I < 154{\cdot}5$, the point x^* is unstable.

TABLE 1

$x_*(I)$ *and* $\lambda_i(I)$ i = 1, 4 (6·3°C)

I	v_*	m_*	n_*	h_*	λ_1, λ_2	λ_3	λ_4
−5	−6·98	0·023	0·218	0·804	−0·251±0·106i	−0·124	−6·08
0	0	0·053	0·318	0·596	−0·203±0·383i	−0·121	−4·68
5	−3·27	0·077	0·369	0·479	−0·097±0·521i	−0·129	−4·60
9	−5·05	0·094	0·397	0·416	−0·015±0·578i	−0·137	−4·73
9·780	−5·35	0·097	0·402	0·406	0±0·586i	−0·138	−4·76
10	−5·43	0·098	0·403	0·403	0·004±0·588i	−0·139	−4·77
20	−8·41	0·135	0·450	0·308	0·155±0·642i	−0·158	−5·28
50	−13·61	0·222	0·530	0·179	0·320±0·715i	−0·204	−6·66
100	−18·46	0·331	0·599	0·104	0·229±0·903i	−0·262	−8·24
150	−21·69	0·413	0·640	0·072	0·020±1·053i	−0·307	−9·33
154·5	−21·94	0·420	0·643	0·070	0±1·063i	−0·311	−9·41
160	−22·24	0·427	0·647	0·068	−0·025±1·075i	−0·315	−9·51
200	−24·19	0·479	0·670	0·055	−0·203±1·138i	−0·346	−10·17
300	−28·12	0·581	0·711	0·036	−0·606±1·172i	−0·412	−11·52

3. Bifurcation Theory

To examine solutions for I near I_k, $k = 1, 2$, we introduce $\mu = I - I_k$, the bifurcation parameter, let:

$$\alpha(\mu) \pm i\omega(\mu),$$

denote the complex conjugate pair of eigenvalues of $J_*(I_k + \mu)$ such that:

$$\alpha(0) = 0, \text{ and let } \omega_0 \equiv \omega(0) > 0.$$

There is a similarity transformation P which reduces $J_*(I_k)$ to the form:

$$P^{-1}J_*(I_k)P = \begin{pmatrix} \begin{pmatrix} 0 & -\omega_0 \\ \omega_0 & 0 \end{pmatrix} & 0 \\ 0 & D \end{pmatrix}, \; D \text{ diagonal.}$$

Specifically, the first two columns of P are the real and imaginary parts of the eigenvector corresponding to the eigenvalue $-i\omega_0$ while the third and fourth columns are the eigenvectors corresponding to the real eigenvalues. With the substitutions:

$$\mathbf{y} = P^{-1}(\mathbf{x} - \mathbf{x}_*),$$

and

$$\mathbf{F}(\mathbf{y}; \mu) = P^{-1}\mathbf{f}(P\mathbf{y} + \mathbf{x}_*, I_k + \mu)$$

the system (1) becomes:

$$\dot{\mathbf{y}} = \mathbf{F}(\mathbf{y}; \mu). \tag{2}$$

For equation (2), the stationary point is the origin.

If $\alpha'(0) \neq 0$, $D_{11} < 0$ and $D_{22} < 0$, a theorem due to Hopf may be applied to demonstrate the existence of small amplitude periodic solutions of (2) for small μ. There is a function $\mu(\varepsilon)$, defined and analytic for all sufficiently small ε, such that $\mu(0) = 0$ and such that equation (2), with $\mu = \mu(\varepsilon)$, has a periodic solution. The solution is unique within the class of nontrivial small amplitude periodic solutions, and has norm $\varepsilon + 0(\varepsilon^2)$. Moreover, the period $T = T(\varepsilon)$ satisfies:

$$\lim_{\varepsilon \to 0} T(\varepsilon) = 2\pi/\omega_0,$$

and the periodic solutions exist for exactly one of the cases $\mu > 0$, $\mu = 0$, $\mu < 0$.

Hopf theory also implies that $\mu(\varepsilon)$ and $T(\varepsilon)$ expand as:

$$\mu(\varepsilon) = \mu_2\varepsilon^2 + 0(\varepsilon^4),$$

and

$$T(\varepsilon) = \frac{2\pi}{\omega_0}[1 + \tau_2\varepsilon^2 + 0(\varepsilon^4)],$$

where μ_2 and τ_2 may be calculated in terms of the partial derivatives of F at the stationary point. The periodic solution of equation (1) expands as:

$$\mathbf{x}(t) = \mathbf{x}_*(I_k) + \varepsilon \operatorname{Re}\,(\exp\,(i\omega_0 t + i\varphi)\mathbf{z}_1] + 0(\varepsilon^2), \quad 0 \leq t \leq T(\varepsilon), \tag{4}$$

where φ is an arbitrary phase angle and $\mathbf{z}_1$ is the eigenvector of $J_*(I_k)$ corresponding to the eigenvalue $i\omega_0$. It is convenient to normalize z_1 such that $(\mathbf{z}_1)_1 = 1$: with this normalization, 2ε is the peak–to–peak amplitude of the voltage v to within $0(\varepsilon^2)$.

The stability of the solution is governed by the associated characteristic exponents. Since $D_{11} < 0$ and $D_{22} < 0$, two of the exponents are negative. By virtue of the "derivative solution", a third exponent vanishes identically. If $\beta(\varepsilon)$ denotes the remaining exponent, then $\beta(\varepsilon)$ expands as:

$$\beta(\varepsilon) = -2\mu_2\alpha'(0)\varepsilon^2 + 0(\varepsilon^4).$$

For small ε, β has the same sign as $-\mu_2\alpha'(0)$. If $\mu_2\alpha'(0) < 0$, the family of periodic solutions is unstable. If $\mu_2\alpha'(0) > 0$, Hopf theory shows that each solution in the family is orbitally asymptotically stable with asymptotic phase as a solution of the full non-linear system.

When used in the context of Hopf theory, the term stable will have the above meaning. Later, in the context of stability analysis by computation of characteristic exponents, the term stable will mean only that the exponents (except for the one that vanishes identically) have negative real parts.

4. The Unstable Oscillations Near $I = I_1$

As described in appendix A, we applied the explicit algebraic formulae for μ_2 and τ_2 given in appendix B to the bifurcation point $I = I_1$.

For $T = 6{\cdot}3°\text{C}$, we found:

$$I_1 = 9{\cdot}780,$$
$$v_* = -5.346, \quad m_* = 0{\cdot}0973,$$
$$n_* = 0{\cdot}402, \quad h_* = 0.406,$$
$$\omega_0 = 0{\cdot}586, \quad \alpha'(0) = 0{\cdot}0188, \quad \omega'(0) = 0{\cdot}00965,$$
$$D_{11} = -0{\cdot}138, \quad D_{22} = -4{\cdot}764$$
$$\mathbf{z}_1 = \begin{pmatrix} 1 \\ -0{\cdot}0103 + 0{\cdot}00183i \\ -0{\cdot}00160 + 0{\cdot}00479i \\ 0{\cdot}00165 - 0{\cdot}00734i \end{pmatrix},$$
$$\mu_2 = -0{\cdot}115 \text{ and } \tau_2 = 0{\cdot}0114.$$

All numbers quoted are rounded to the number of digits shown, and all digits are believed to be correct.

Interpreting these numbers, since:

$$I - I_1 = \mu_2 \varepsilon^2 + 0(\varepsilon^2),$$

and $\mu_2 < 0$, the small periodic solutions occur for values of I less than I_1. Since $\alpha'(0)\mu_2 < 0$, the oscillations are unstable.

For $I \approx I_1$, $I < I_1$, the oscillations are basically circles about the stationary point and in the plane spanned by the real and imaginary parts of $\mathbf{z}_1$. In approximate terms, if the system is started in this plane with the initial point inside the circle of radius $((I-I_1)/\mu_2)^{\frac{1}{2}}$, the solution decays in an oscillatory manner to the rest state. If the initial point is outside this circle, the amplitude grows, the solution leaves the plane and is observed numerically to wind onto the well-known large amplitude stable periodic solution.

If the system is started off the plane, the behaviour of the solution will depend upon the component of the initial conditions that does lie in the plane.

The numerical integration scheme described in appendix C was also employed to investigate the unstable oscillations for $I < I_1$. The amplitude and period of the oscillations found numerically are compared with those predicted by the equations:

$$\varepsilon \approx [(I-I_1)/\mu_2]^{\frac{1}{2}}$$

$$T \approx \frac{2\pi}{\omega_0}(1+\tau_2\varepsilon^2)$$

in Table 2. As expected, the agreement between the two approaches improves as $I \to I_1$.

Figure 1 shows both the unstable oscillation discussed here and the large amplitude stable oscillation for $I = 8$. The unstable oscillation has evolved from a sine wave at $I \approx 9{\cdot}78$ into the triangular form shown.

TABLE 2

Unstable oscillations

I	v_{pp}	$2((I-I_1)/\mu_2)^{\frac{1}{2}}$	T	$2\pi(1+\tau_2\varepsilon^2)/\omega$
9·780	—	0	—	10·718
9·77	0·58	0·58	10·728	10·728
9·7	1·68	1·66	10·803	10·802
9·6	2·54	2·50	10·914	10·907
9·5	3·21	3·11	11·030	11·013
9·0	5·74	5·20	11·699	11·540
8·5	8·14	6·66	12·622	12·067
8·0	11·8	7·85	14·377	12·595

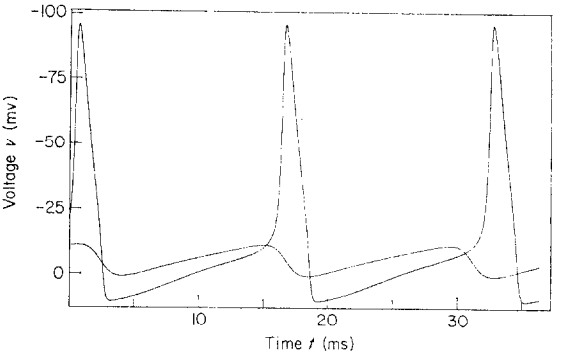

FIG. 1. Voltage oscillations for $I = 8\ \mu\text{A cm}^{-2}$.

For $T = 0°\text{C}$, the bifurcation theoretic approach gave:

$$I_1 = 8{\cdot}418,$$
$$v_* = -4{\cdot}816, \quad m_* = 0{\cdot}0918,$$
$$n_* = 0{\cdot}393, \quad h_* = 0{\cdot}425,$$
$$\omega_0 = 0{\cdot}360, \quad \alpha'(0) = 0{\cdot}0146, \quad \omega'(0) = 0{\cdot}00466,$$
$$D_{11} = -0{\cdot}0680, \quad D_{22} = -2{\cdot}982,$$
$$\mathbf{z}_1 = \begin{pmatrix} 1 \\ -0{\cdot}00967 + 0{\cdot}00206i \\ -0{\cdot}00108 + 0{\cdot}00401i \\ 0{\cdot}00110 - 0{\cdot}00608i \end{pmatrix},$$
$$\mu_2 = -0{\cdot}0833 \text{ and } \tau_2 = 0{\cdot}0149.$$

The situation is not much different than at 6·3°C. The critical value of the stimulus I, is lower, the unstable oscillations are slower, and the amplitude of the unstable oscillations grows somewhat faster as I is decreased from I_1. Decreasing the temperature did not "turn the bifurcation around".

5. The Stable Oscillations Near $I = I_2$

When we applied the bifurcation formulae to the point $I = I_2$, we found:

$$I_2 = 154{\cdot}53,$$
$$v_* = -21{\cdot}94, \quad m_* = 0{\cdot}420,$$
$$n_* = 0{\cdot}643, \quad h_* = 0{\cdot}0704,$$
$$\omega_0 = 1{\cdot}063, \quad \alpha'(0) = -0{\cdot}00449, \quad \omega'(0) = 0{\cdot}00220,$$
$$D_{11} = -0{\cdot}311, \quad D_{22} = -9{\cdot}412,$$

$$\mathbf{z}_1 = \begin{pmatrix} 1 \\ -0{\cdot}0207 \quad +0{\cdot}0108i \\ -0{\cdot}000715 + 0{\cdot}00286i \\ 0{\cdot}000693 - 0{\cdot}00222i \end{pmatrix},$$

$\mu_2 = -0{\cdot}280$ and $\tau_2 = 0{\cdot}000453$.

Just as in section 4, since:

$$I - I_2 = \mu_2 \varepsilon^2 + 0(\varepsilon^4)$$

and $\mu_2 < 0$, the small periodic solutions occur for values of I less than I_2. Since $\alpha'(0)\mu_2 > 0$, the oscillations are stable.

These stable oscillations are precisely those observed numerically by a variety of authors. It is interesting to note that an attempt was made (Sabah & Spangler, 1970) to describe the oscillations by "analytic" means: the technique of harmonic balancing was employed, and a good description of the amplitude was obtained. In the light of the present application of bifurcation theory, this attempt was somewhat naïve as indicated by the failure to predict the period of the solutions.

Careful numerical integrations of the stable oscillations were undertaken for values of I near I_2 in order to provide numerical results of sufficient accuracy for comparison with bifurcation theory. The comparison is given in Table 3. Again, as expected, the agreement between the two approaches improves as $I \to I_2$.

TABLE 3

Stable oscillations

I	v_{pp}	$2((I - I_2)/\mu_2)^{\frac{1}{2}}$	T	$2\pi(1 + \tau_2\varepsilon^2)/\omega_0$
154·53	—	0	—	5·911
154·4	1·35	1·35	5·912	5·912
154	2·74	2·74	5·916	5·916
152	6·08	6·01	5·936	5·935
150	8·22	8·04	5·958	5·955
145	12·2	11·7	6·016	6·002
135	18·6	16·7	6·153	6·098
120	27·5	—	6·400	—
100	40·5	—	6·784	—
75	58·4	—	7·46	—
50	76·9	—	8·54	—
25	95·2	—	10·75	—
15	102·3	—	12·72	—
10	105·3	—	14·64	—
8	106·1	—	16·01	—
7	105·9	—	17·15	—
6·5	105·1	—	18·17	—

At $I = I_2$, for $T = 0°C$, we calculated:

$$I_2 = 152.30,$$
$$v_* = -21.82, \quad m_* = 0.416,$$
$$n_* = 0{\cdot}642, \quad h_* = 0{\cdot}0713,$$
$$\omega_0 = 0{\cdot}566, \quad \alpha'(0) = -0{\cdot}00262, \quad \omega'(0) = 0{\cdot}000966$$
$$D_{11} = -0{\cdot}155, \quad D_{22} = -8{\cdot}189,$$
$$\mathbf{z}_1 = \begin{pmatrix} 1 \\ -0{\cdot}0201 \quad +0{\cdot}0112i \\ -0{\cdot}000635 + 0{\cdot}00270i \\ 0{\cdot}000618 - 0{\cdot}00212i \end{pmatrix},$$
$$\mu_2 = -0{\cdot}271 \text{ and } \tau_2 = 0{\cdot}000498.$$

The most evident result of the decreased temperature is slower oscillations, however the bifurcation phenomenon is essentially the same as at 6·3°C.

6. The Stable–Unstable Bifurcation at $I = I_0$

After investigating the small stable oscillations for I near I_2, we computed the family of stable oscillations for smaller values of I. The shooting technique described in appendix C was employed, with the initial estimates provided by quadratic extrapolation of points on previously computed orbits. The parameter I was used as the extrapolation variable until the amplitude of the computed oscillation began to decrease with smaller values of I. Then the amplitude itself was used as the extrapolation variable.

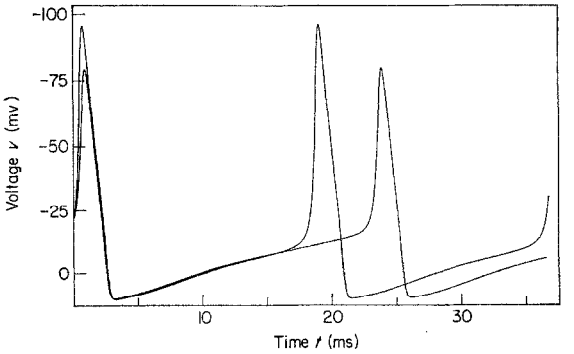

FIG. 2. Voltage oscillations for $I = 6{\cdot}48\ \mu\text{Acm}^{-2}$.

With careful extrapolation, we were able to extend the computation around the point of vertical tangency at $I = I_0$ in Fig. 3. For values of $I \approx I_0$, $I > I_0$, we thus computed two distinct periodic solutions. Figure 2 shows one such pair, for $I = 6{\cdot}48$.

By fitting a cubic to I as a function of v_{pp}, we found $I_0 = 6{\cdot}265$ for an amplitude $v_{pp} = 101{\cdot}78$.

To investigate the stability of the pair of large periodic solutions, we computed the characteristic exponents associated with the solutions as in appendix C. This computation is a linear stability analysis. Of the four exponents, one vanishes identically and two are strictly negative. The remaining exponent, β, is given in Table 4.

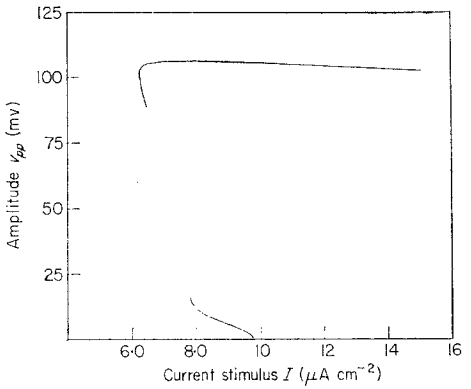

FIG. 3. Peak to peak voltage vs. current stimulus.

TABLE 4

Stable-unstable bifurcation

I	v_{pp}	T	β
6·48	105·0	18·24	−0·112
6·4	104·6	18·53	−0·098
6·3	103·6	19·13	−0·061
6·2718	102·70	19·53	−0·031
6·2655	102·14	19·78	−0·012
6·2648	101·98	19·82	−0·006
6·2648	101·57	19·97	0·007
6·2655	101·38	20·04	0·013
6·2718	100·57	20·31	0·039
6·3	98·6	20·90	0·100
6·4	92·9	22·18	0·244
6·48	88·5	22·92	0·334

As $I \to I_0$, the stable larger amplitude solution and the unstable smaller amplitude solution coalesce into a single solution for which $\beta = 0$.

The differences in amplitude and period of the pair of solutions appear to exhibit the behaviour of the form

$$\text{const.}\ (I - I_0)^{\frac{1}{2}}.$$

The reason β vanishes at $I = I_0$ may be explained as follows. Let $x_1(t;I)$, $x_2(t;I)$ denote the pair of coalescing solutions with phases adjusted so that:

$$[x_1(0; I)]_1 = [x_2(0; I)]_1 = \text{const.},$$

as (for example) in Fig. 2. Let $z(t;I)$ denote the difference $x_1(t;I) - x_2(t;I)$ normalized in such a manner that:

$$\lim_{I \to I_0} z(t; I) \equiv z_0(t)$$

is well-defined.

If we let $x_0(t)$ denote the limit:

$$x_0(t) = \lim_{I \to I_0} x_1(t; I) = \lim_{I \to I_0} x_2(t; I),$$

then both $z = z_0$ and $z = \dot{x}_0$ are periodic solutions of the variational equation:

$$\dot{z} = f_x[x_0(t); I_0]z.$$

If $z_0(0)$ and $\dot{x}_0(0)$ are independent, two characteristic exponents must vanish. Numerically, (at least) it is easy to verify that $[\dot{x}_0(0)]_1 \neq 0$, so this last assumption is valid.

In an attempt to "join up" the branches of the bifurcation diagram (Fig. 3), we computed progressively smaller amplitude periodic solutions for larger values of I. The scheme broke down, however, as the solutions became more unstable and it was necessary to continually reduce the amount of the extrapolation so that the shooting scheme would converge from the extrapolated point. There was no difficulty with convergence once an accurate initial guess had been obtained.

7. The Unstable–Unstable Bifurcation at $I = I_3$

After investigating the small amplitude unstable oscillations for I near I_1, we proceeded to compute larger amplitude unstable oscillations for smaller values of I in an attempt to "join up" with the large amplitude unstable oscillations of section 6. Quadratic extrapolation with the computed amplitude as the extrapolation variable was employed as in section 6. The scheme

ultimately failed when the shooting procedure failed to converge to adequate accuracy despite the numerical integrations being performed at limiting precision.

Before the breakdown occurred, however, we found an unanticipated bifurcation at $I = I_3 = 7{\cdot}8466$ as shown in Table 5. For values of $I \approx I_3$, $I > I_3$, there are a pair of distinct periodic solutions which coalesce into a single solution of amplitude $v_{pp} = 16{\cdot}17$ as $I \to I_3$.

TABLE 5

Unstable–unstable bifurcation

I	v_{pp}	T
7·9500	12·428	14·719
7·9000	13·352	15·205
7·8779	13·945	15·519
7·8550	14·954	16·057
7·8500	15·381	16·284
7·8480	15·658	16·431
7·8470	15·894	15·557
7·8468	15·973	16·599
7·8467	16·027	16·627
7·8467	16·32	16·78
7·8468	16·38	16·81
7·8470	16·40	16·82

According to the argument of section 6, one of the three non-zero characteristic exponents vanishes at $I = I_3$. For the smaller amplitude solution of the coalescing pair, two exponents are negative, and one is positive. (see section 4).

We were unable to compute the larger amplitude solutions with sufficient accuracy to further compute the characteristic exponents. For $I = 7{\cdot}85$, however, we computed $\beta = 0{\cdot}22$ for the smaller amplitude solution so it is fairly clear that the positive exponent associated with the smaller solution is not the exponent that is vanishing. Therefore one of the negative exponents must vanish and (presumably) become positive when associated with the larger solution. The largest positive exponent carries over as positive, so the larger amplitude solution of the coalescing pair is unstable by virtue of two positive characteristic exponents.

The bifurcation at $I = I_3$ is therefore of unstable–unstable type, and is not of physical interest. Mathematically, however, the bifurcation diagram for the Hodgkin–Huxley model is more complicated than expected. If we assume that the branches in Fig. 3 do indeed join up, there must be at least

one more unstable–unstable bifurcation at some value of I, say $I = I_4$ where $I_4 > I_3$. In terms of periodic solutions, it appears that for $I \approx I_3$, $I > I_3$ there are (at least) five periodic solutions of the system.

5. Discussion

The present study confirms the suggestion first made by Cooley, Dodge & Cohen (1965) that the repetitive behaviour of the current clamped Hodgkin–Huxley system for small current stimuli is a "hard" oscillation. Of the unstable periodic solutions we discuss, the small oscillations for $I \approx I_1$ are the most interesting because they represent the mechanism whereby the perturbed physiological system either returns to the stable rest state or exhibits larger oscillations.

Figure 1 shows both the unstable periodic solution and the stable periodic train of action potentials for a current stimulus $I = 8\mu\text{A cm}^{-2}$. Intuitively, one might expect that oscillations of smaller amplitude than the unstable oscillation will decay to the stable stationary state. Since the system is four-dimensional rather than two-dimensional, this notion is not correct although it contains some truth.

The unstable periodic solution describes a closed trajectory on the two-dimensional center manifold (Hassard & Wan, 1977) for the system. If, under the center manifold restriction a point in four-dimensions is mapped into the interior of the set bounded by the closed trajectory, then that point represents the initial conditions for a decaying solution. The larger the amplitude of the unstable periodic solution, the larger the interior of the set on the center manifold and the larger the set of initial conditions which produce decaying solutions.

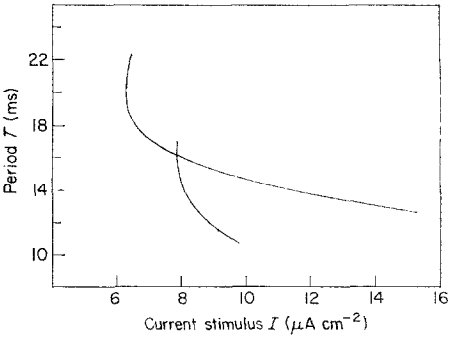

FIG. 4. Period vs. current stimulus.

For the Hodgkin–Huxley system, the numerics suggest that all solutions are either periodic or tend to one of the two stable periodic solutions, namely the stationary point and the train of action potentials. This observation still remains conjecture.

Figures 3 and 4 pose interesting questions. The gap in the bifurcation diagram very probably contains at least one more point of vertical tangency. Similarly, the graph of the periods is expected to connect in some fashion. It is even conceivable that the branches of the period might meet at infinity.

This work was inspired by S P Hastings, and originally employed the Hsu-Kazarinoff formula for μ_2 (Hsu & Kazarinoff, 1976). The formula for τ_2 is due to Y H Wan (Hassard & Wan, 1977), who very kindly derived the formula at the author's request for the present application. Thanks are also due to J. Boa for helpful discussions.

REFERENCES

Cooley, J., Dodge, F. & Cohen, H. (1965). *J. cell comp. Physiol.* **66,** 99.
Hassard, B. D. & Wan, Y. H. (1977). *J. Math. Anal. Appln.* to appear.
Hodgkin, A. L. & Huxley, A. F. (1952). *J. Physiol.* **117,** 500.
Hsu, I. D. & Kazarinoff, N. D. (1976). *J. Math. Anal. Appln.* **55,** 61.
Sabeth, N. H. & Spangler, R. A. (1970). *J. theor. Biol.* **29,** 155.
Troy, W. C. (1974). Oscillatory Phenomena in Nerve Conduction Equations, Ph.D. Dissertation, SUNY at Buffalo.

APPENDIX A

The Bifurcation Calculation

The main difficulty in application of bifurcation formulae to systems of any order is the sheer algebraic complexity of the computation. The present analysis is perhaps the most complex application of bifurcation formulae to date. We owe our success in part to the extensive use of symbolic manipulation to perform the tedious algebra, and in part to the use of recently derived "applicable" bifurcation formulae.

Analytic expressions for the partial derivatives:

$$\frac{\partial f^l}{\partial x_i}, \frac{\partial^2 f^l}{\partial x_i \partial x_j}, \frac{\partial^3 f^l}{\partial x_i \partial x_j \partial x_k}, \quad i, j, k, l = 1, \ldots, 4$$

were calculated with an 80 card SYMBAL program. Formulae output from this program were translated into FORTRAN with a short SNOBOL program. These expressions left the derivatives $\alpha_q^{(j)}$, $\beta_q^{(j)}$, $j = 1, 2, 3$, $q = m, n, h$

arbitrary. Analytic expressions for the derivatives of the functions:

$$\alpha_q(v), \beta_q(v), \quad q = m, n, h$$

in terms of the functions exp, expc, and the derivatives of expc were calculated with a 45 card SYMBAL program, and again translated into FORTRAN.

The end product of the automatic manipulations and translations was a FORTRAN subroutine to evaluate the partial derivatives of $\mathbf{f}$ up to third order in terms of closed form, analytic expressions. To verify the subroutine, for $k = 0, 1, 2$ we computed approximations to the $k+$ first order partial derivatives by differencing the k'th order partial derivatives as computed from the analytic expressions. We then compared the $k+$first order partial derivatives as computed according to the analytic formulae to the finite difference approximations.

In the following, we describe the calculations at the bifurcation point I_1. We later indicate how the calculation at I_2 differed.

If one chooses to regard v_* rather than I as the bifurcation parameter, one may obtain closed form analytic expressions (cfe's) for the eigenvalues of the 4×4 matrix $\mathbf{J}_*(I)$ in terms of v_*. Thus there are cfe's for ω_0 and for the elements of P and P^{-1} in terms of $v_1 = v_*(I_1)$. Except for P_{12}, however, no elements of either P of P^{-1} vanish identically, so that the cfe's for the derivatives of $\mathbf{F}$ involve essentially every non-zero derivative of $\mathbf{f}$ of the same order. In addition, the calculation in terms of cfe's breaks down when it comes to expressing v_1 as cfe in terms of the other parameters of the problem.

We therefore used the analytic expressions for the derivatives of $\mathbf{f}$ to calculate numbers, and found v_1, ω_0, P, P^{-1}, the derivatives of $\mathbf{F}$ and hence μ_2 and τ_2 as numbers.

The QR algorithm was employed to calculate the eigenvalues.

$$\lambda_i(v_*), \quad i = 1, \ldots, 4$$

of $\mathbf{J}_*$ for different values of v_*. The eigenvalues were ordered so that their real parts obeyed:

$$\lambda_i^r \geq \lambda_{i+1}^r, \quad i = 1, 2, 3.$$

Müllers method was used to zero $\lambda_1^r(v_*)$ and determine v_1 such that $\lambda_1^r(v_1) = 0$. We then set $\omega_0 = \lambda_1^i(v_1)$. To calculate $\alpha'(0)$, we differenced λ_1^r and $I = -g(v_*)$ at $v_* = v_1$.

The matrix $\mathbf{P}$ was formed as:

$$\mathbf{P} = [(\mathbf{z}_1^r)(-\mathbf{z}_1^i)(\mathbf{z}_3)(\mathbf{z}_4)],$$

where $\mathbf{z}_i$ $i = 1, \ldots, 4$ are the eigenvectors of $\mathbf{J}_*(I_1)$, normalized so as to have first components unity. The inverse P^{-1} was calculated explicitly and

the inverse was verified by direct multiplication. The product $P^{-1}\mathbf{J}_*(I_1)P$ was formed, and was observed to possess the desired canonical form. The partial derivatives of $\mathbf{f}$ were all calculated at $v_* = v_1$ $(I = I_1)$, and the derivatives of $\mathbf{F}$ were calculated from them using P and P^{-1}. To verify the conversion of $\mathbf{f}$ derivatives to $\mathbf{F}$ derivatives, the conversion was inverted.

Finally, the formulae listed in appendix B were used to evaluate μ_2 and τ_2. At the second bifurcation point, $I = I_2$, the same calculations outlined above were performed, except that the initial guess in the root-finding process to zero λ_1^r as a function of v_* was taken close to v_2.

Note: Recently, the author has developed a program for the numerical evaluation of bifurcation formulae for N dimension systems of autonomous o.d.e.'s $N \leq 20$. This program requires cfe's only for the functions and Jacobian matrix of the original system. Numerical differentiation is employed to evaluate the required third partial derivatives.

APPENDIX B

Formulae for μ_2 and τ_2

Following Hassard & Wan (1977), we have:

$$\mu_2 = -\operatorname{Re} c_1(0)/\alpha'(0),$$

and

$$\tau_2 = -[\operatorname{Im} c_1(0) + \mu_2\omega'(0)]/\omega_0,$$

where:

$$\begin{aligned}
c_1(0) &= \frac{i}{2\omega_0}(g_{20}g_{11} - 2g_{11}\bar{g}_{11} - g_{02}\bar{g}_{02}/3) + \frac{g_{21}}{2},\\
g_{20} &= \tfrac{1}{4}[F^1_{20} - F^1_{02} + 2F^2_{11} + i(F^2_{20} - F^2_{02} - 2F^1_{11})],\\
g_{11} &= \tfrac{1}{4}[F^1_{20} + F^1_{02} + i(F^2_{20} + F^2_{02})]\\
g_{02} &= \tfrac{1}{4}[F^1_{20} - F^1_{02} - 2F^2_{11} + i(F^2_{20} - F^2_{02} + 2F^1_{11})],\\
g_{21} &= \tfrac{1}{8}[F^1_{30} + F^1_{12} + F^2_{21} + F^2_{03} + i(F^2_{30} + F^2_{12} - F^1_{21} - F^1_{03})] +\\
&\quad + [F^{1,1}_{10} + F^{2,1}_{01} + i(F^{2,1}_{10} - F^{1,1}_{01})]w_{11} +\\
&\quad + \tfrac{1}{2}[F^{1,1}_{10} - F^{2,1}_{01} + i(F^{1,1}_{01} + F^{2,1}_{10})]w_{20},\\
w_{20} &= -\tfrac{1}{4}(D - 2i\omega_0)^{-1}(\hat{F}_{20} - \hat{F}_{02} - 2i\hat{F}_{11}),
\end{aligned}$$

and

$$w_{11} = -\tfrac{1}{4}D^{-1}(\hat{F}_{20} + \hat{F}_{02}).$$

In the above,

$$F^i_{jk} = \left(\frac{\partial}{\partial y_1}\right)^j \left(\frac{\partial}{\partial y_2}\right)^k F^i,$$

$$F^{i,1}_{jk} = \left(\frac{\partial F^i_{jk}}{\partial y_3}, \frac{\partial F^i_{jk}}{\partial y_4}\right), \quad i = 1, \ldots, 4$$

and

$$\hat{F}_{ij} = (F^3_{ij}, F^4_{ij})^t.$$

The partial derivatives of $\mathbf{F}(\mathbf{y})$ are calculated in terms of the partial derivatives of $\mathbf{f}(\mathbf{x})$ by means of the relationships:

$$\frac{\partial \mathbf{F}}{\partial y_i} = P^{-1} \sum_{r=1}^{4} P_{ri} \frac{\partial \mathbf{f}}{\partial x_r},$$

$$\frac{\partial^2 \mathbf{F}}{\partial y_i \partial y_j} = P^{-1} \sum_{r,s=1}^{4} P_{ri} P_{sj} \frac{\partial^2 \mathbf{f}}{\partial x_r \partial x_s},$$

and

$$\frac{\partial^3 \mathbf{F}}{\partial y_i \partial y_j \partial y_k} = P^{-1} \sum_{r,s,t=1}^{4} P_{ri} P_{sj} P_{tk} \frac{\partial^3 \mathbf{f}}{\partial x_r \partial x_s \partial x_t}.$$

APPENDIX C

The Integration Schemes

Consider the system (1), i.e.

$$\frac{\mathrm{d}\mathbf{x}}{\mathrm{d}t} = \mathbf{f}(\mathbf{x}).$$

Assume the existence of a non-stationary periodic solution $\mathbf{p}(t)$, and let $\mathbf{x}_0$ denote an initial guess of some point belonging to the orbit of $\mathbf{p}$.

It is essential to the scheme that x^1_0, the first component of $\mathbf{x}_0$, satisfies:

$$\min_t p^1(t) < x^1_0 < \max_t p^1(t).$$

It is also extremely important that $\mathbf{x}_0$ be a good guess, since a Newton–style iteration will be performed with the components x^j_0 $j = 2, \ldots, 4$ as the initial estimate.

The calculation described in this paragraph will be called "integrating around once". Apply the variable order variable step size Gear algorithm for stiff systems to the system with initial conditions $\mathbf{x}(0) = \mathbf{x}_0$, noting the sign of $\mathrm{d}x^1/\mathrm{d}t(0)$. Continue the integration until $t = T_1$ such that:

$$x^1(T_1) = x^1(0),$$

and

$$\operatorname{sgn}\frac{dx^1}{dt}(T_1) = \operatorname{sgn}\frac{dx^1}{dt}(0).$$

Interpolate to obtain values for:

$$x^j(T_1), \quad j = 2, 3, 4.$$

Let:

$$\psi = (\psi^1, \ldots, \psi^3),$$

denote the vector-valued function of the variable:

$$\eta = (\eta^1, \ldots, \eta^3),$$

defined as follows. Let:

$$x_0^{j+1} = \eta^j, \quad j = 1, \ldots, 3,$$

integrate around once, and let:

$$\psi^{j+1} = x^{j+1}(T_1) - x_0^{j+1}, \quad j = 1, \ldots, 3.$$

The problem of computing periodic orbits of the four-dimensional system becomes one of solving the system of three simultaneous non-linear equations in three unknowns represented by:

$$\psi(\eta) = \mathbf{0}.$$

To this system, we applied a Newton method in which the Jacobian $\partial\psi^i/\partial n_j$ was evaluated by differencing. Four integrations around were required for each iterative step.

Both the convergence of the shooting scheme and the ultimate accuracy of the computed solution depend upon the bound specified for the single step error. The convergence also depends upon the quantities $\delta_j = 1, 2, 3$ used to estimate the Jacobian of the map $\psi(\eta)$ by means of:

$$\frac{\partial\psi_i}{\partial\eta_j} \approx \frac{\psi_i(\eta + \delta_j\hat{e}_j) - \psi_i(\eta)}{\delta_j}.$$

The computations were performed in single precision (14 decimal digits) on CDC 6400 and CDC Cyber 173 machines. Values for the single step error and the quantities δ_j were determined by numerical experimentation and were adjusted so that in general, at least seven digits in the computed solution were correct.

(A) CALCULATION OF CHARACTERISTIC MULTIPLIERS

The values of β listed in Table 4 were computed as follows.

First, the shooting scheme described above was employed to calculate the periodic orbit to especially high precision. Then eight further numerical integrations were performed, from $t = 0$ to up to the period T calculated

above, initial conditions:

$$\mathbf{x}_0 \pm \delta_j \hat{e}_j, \quad j = 1, \ldots, 4.$$

Let $\mathbf{X}(\mathbf{x}_0 + \delta_j \hat{e}_j)$ denote the values of these solutions at time T. We formed the matrix:

$$\mathbf{A}_{ij} = \frac{X_i(\mathbf{x}_0 + \delta_j \hat{e}_j) - X_i(\mathbf{x}_0 - \delta_j \hat{e}_j)}{2\delta_j}$$

and calculated its eigenvalues using the QR algorithm.

The eigenvalues of $\mathbf{A}$ approximate the characteristic multipliers associated with the periodic solution. One of the characteristic multipliers is identically one. This fact was used to check the accuracy of the calculation and to determine appropriate values for the δ_j's $j = 1, \ldots, 4$. After identifying the characteristic multiplier m corresponding to the exponent β, we calculated β as:

$$\beta = \log(m)/T.$$

Note: The scheme just outlined is not able to calculate the more negative exponents with accuracy. To accomplish this task, a more refined scheme is required.